NeuroImage 147 (2017) 79–88

Contents lists available at ScienceDirect

NeuroImage

journal homepage: www.elsevier.com/locate/neuroimage

A streamlined acquisition for mapping baseline brain oxygenation using quantitative BOLD

Alan J. Stone*, Nicholas P. Blockley

FMRIB Centre, Nuffield Department of Clinical Neurosciences, University of Oxford, Oxford, UK

A B S T R A C T

Quantitative BOLD (qBOLD) is a non-invasive MR technique capable of producing quantitative measurements of the haemodynamic and metabolic properties of the brain. Here we propose a refinement of the qBOLD methodology, dubbed streamlined-qBOLD, in order to provide a clinically feasible method for mapping baseline brain oxygenation. In streamlined-qBOLD confounding signal contributions are minimised during data acquisition through the application of (i) a Fluid Attenuated Inversion Recovery (FLAIR) preparation to remove cerebral spinal fluid (CSF) signal contamination, (ii) a Gradient Echo Slice Excitation Profile Imaging (GESEPI) acquisition to reduce the effect of macroscopic magnetic field gradients and (iii) an Asymmetric Spin Echo (ASE) pulse sequence to directly measure the reversible transverse relaxation rate, R_2'. Together these features simplify the application of the qBOLD model, improving the robustness of the resultant parametric maps. A theoretical optimisation framework was used to optimise acquisition parameters in relation to signal to noise ratio. In a healthy subject group (n = 7) apparent elevations in R_2' caused by partial volumes of CSF were shown to be reduced with the application of CSF nulling. Significant decreases in R_2' ($p < 0.001$) and deoxygenated blood volume ($p < 0.01$) were seen in cortical grey matter, across the group, with the application of CSF suppression. Quantitative baseline brain oxygenation parameter maps were calculated using qBOLD modelling and compared with literature values.

1. Introduction

Techniques capable of providing quantitative maps of baseline brain oxygenation provide valuable information about the metabolic profile of brain tissue and have clinical applications in diseases such as stroke (Yamauchi et al., 1996), cancer (Leenders, 1994) and neurodegenerative disorders (Ishii et al., 1996; Borghammer et al., 2012). However, to date available options for mapping brain oxygenation have been limited. The current benchmark for quantifying and mapping brain oxygenation is triple oxygen PET (Ito et al., 2005). Unfortunately, this technique is highly specialised, invasive, expensive and difficult to perform. Therefore, there is a clear need for a clinically relevant alternative, capable of mapping the regional and spatial extent of brain oxygenation in a non-invasive, quantitative fashion.

One potential alternative is the quantitative BOLD (qBOLD) method. It is a non-invasive MRI based technique that is capable of producing quantitative measurements of the haemodynamic and metabolic properties of the brain on a regional basis (Yablonskiy et al., 2013). This is achieved by modelling the transverse MR signal decay in the presence of a vascular network by exploiting the sensitivity to deoxygenated blood of the reversible transverse relaxation rate R_2' (where $R_2'=R_2^*- R_2$) (He and Yablonskiy, 2007). To describe the qBOLD model in simple terms, the mono-exponential part of the signal decay is used to measure R_2'. The mismatch between a measured spin echo and the linear intercept of the mono-exponential regime provides an estimate of the deoxygenated blood volume (DBV) (see Fig. 1) (Yablonskiy, 1998). These measurements can then be combined to estimate the oxygen extraction fraction (OEF), a quantitative measure of baseline brain oxygenation.

Although qBOLD is a promising approach, in practice it suffers from a number of limitations or confounds. It is heavily reliant on an accurate measurement of R_2' which can become elevated in the presence of macroscopic magnetic field gradients (MFGs), particularly around air-tissue interfaces. Left uncorrected this will result in confounded estimates of OEF. Additionally, the original qBOLD implementation acquired R_2'-weighted images with varying amounts of R_2-weighting and separating these effects is problematic. Furthermore, the presence of partial volumes of cerebrospinal fluid (CSF) must be accounted for, which would otherwise result in an overestimated measurement of R_2' (He and Yablonskiy, 2007; Dickson et al., 2009;

* Correspondence to: FMRIB Centre, Nuffield Department of Clinical Neurosciences, University of Oxford, John Radcliffe Hospital, Headington, Oxford OX3 9DU, UK.
E-mail address: alan.stone@ndcn.ox.ac.uk (A.J. Stone).

http://dx.doi.org/10.1016/j.neuroimage.2016.11.057
Received 14 July 2016; Received in revised form 8 October 2016; Accepted 22 November 2016
Available online 30 November 2016
1053-8119/

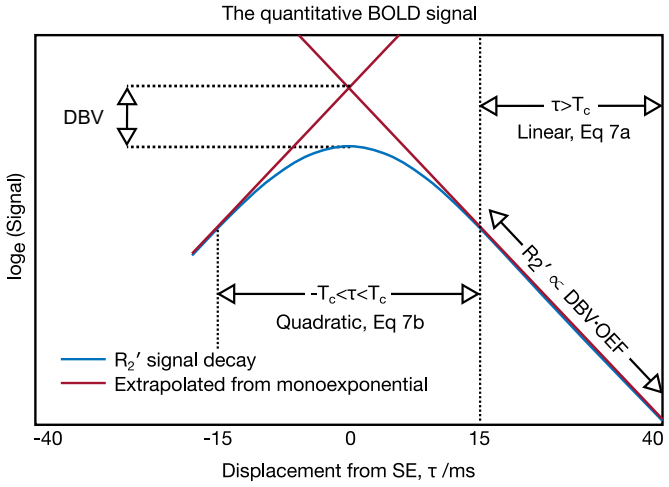

Fig. 1. Schematic of the qBOLD model describing the transverse MR signal decay in the presence of a blood vessel network. R_2' is inferred from the monoexponential regime (where $\tau > T_c$ (Eq. (7)) and T_c=1.5 t_c (Eq. (6)) where t_c is the characteristic time) and DBV inferred from the mismatch between the linear intercept of this fit and spin echo signal (τ = 0 ms). Combining these two measurements estimates of baseline brain oxygenation can be made (Eqs. (11) and (12)).

Simon et al., 2016). Whilst MFGs were corrected using a separately acquired magnetic field map, the effects of R_2-weighting and CSF partial volumes were accounted for by using a compartmental model. This led to an over-parameterisation of the model requiring high signal to noise (SNR) in order to make accurate quantification of brain oxygenation (Christen et al., 2011).

In this study we propose a refinement of the qBOLD methodology in order to progress towards a clinically feasible method for mapping baseline brain oxygenation. A novel acquisition protocol is used to remove confounding effects from the measurement of R_2' and improve the robustness of the resultant parametric maps. The limitations of the original qBOLD implementation are addressed in the following ways. Firstly, an asymmetric spin echo (ASE) pulse sequence is used to provide a direct measure of R_2' (Wismer et al., 1988), eliminating the need to remove R_2-weighting from the acquired signal. This is possible with ASE because images are acquired at the same echo time (TE) resulting in the same degree of R_2-weighting, but with the level of R_2'-weighting manipulated by shifting the spin echo refocussing pulse by an amount $\tau/2$. By repeating this process for a number of different values of the spin echo displacement time, τ, a measurement of R_2' can be made. ASE has previously been implemented with qBOLD modelling to provide parametric maps of baseline brain oxygenation (An and Lin, 2003). Secondly, in contrast to previous qBOLD implementations, we propose to compensate for MFGs prospectively rather than through postprocessing. The Gradient Echo Slice Excitation Profile Imaging (GESEPI) technique aims to compensate for MFGs by oversampling in the slice direction using a 3D acquisition (Yang et al., 1998). We have recently shown that by combining GESEPI with the ASE technique (GASE) the effect of MFGs can be minimised in the majority of the brain (Blockley and Stone, 2016). Finally, the signal contribution of CSF can be removed through the use of a FLAIR (Fluid Attenuated Inversion Recovery) preparation pulse (Hajnal et al., 1992). This has been shown to reduce the overestimation of R_2' seen in voxels with a high CSF fraction (Dickson et al., 2009; Simon et al., 2016). Taken together these modifications to the acquisition of R_2'-weighted data enable the signal model to be simplified.

In summary, the proposed FLAIR-GASE method uses an ASE measurement of R_2', GESEPI acquisition and FLAIR CSF suppression to minimise the confounds in the acquired signal. In turn a simple model of the qBOLD signal was used to analyse this data, with the aim of further simplifying the implementation of the qBOLD method. The ultimate aim of this work is to provide a clinically relevant and robust approach to mapping baseline brain oxygenation which is non-invasive, requires no additional equipment, is easy to implement and feasible to acquire in a short scan time.

2. Theory

2.1. FLAIR-GASE optimisation

Optimisation of the FLAIR-GASE pulse sequence was performed to minimise the signal contribution of CSF and maximise the SNR of the measurement of R_2'. The FLAIR preparation uses an inversion pulse to separate the signal contributions in a voxel by their T_1 value. An appropriate inversion time (TI) must be chosen such that the CSF signal is nulled taking into account the effects of the repetition time (TR) (Shen et al., 2009).

$$TI = T_1 \log\left(\frac{2}{1+e^{-TR/T_1}}\right) \quad (1)$$

Optimisation of the ASE pulse sequence was adapted from *Gowland and Bowtell* (Gowland and Bowtell, 2007), where the acquisition of multi-echo FMRI data was optimised and *Song and Song* (R. Song and H. K. Song, 2007), where echo-spacing was optimised for the simultaneous measurement of R_2 and R_2'. Here we adapt this approach to optimise the acquisition of multi-τ-weighted ASE data for the measurement of R_2'. The signal acquired for the j^{th} τ-weighted ASE acquisition is given by Eq. (2), where J is the total number of τ-weighted data-points acquired and j=1, 2, ..., J.

$$S_j = S_0 . e^{-TE.R_2} e^{-\tau_j R_2'} \quad (2)$$

The degree of R_2'-weighting in an ASE sequence is determined by the spin echo displacement time, τ. Under the assumption of an ideal ASE sequence whereby pulses are instantaneous and may overlap, the minimum value of τ, τ_{min}, is 0 ms and the maximum is determined by TE i.e. τ_{max}=TE. Given a linear distribution of τ values between τ_{min} and τ_{max} each acquired in a separate repetition (see Fig. 2), values of τ_j can be defined by Eq. (3).

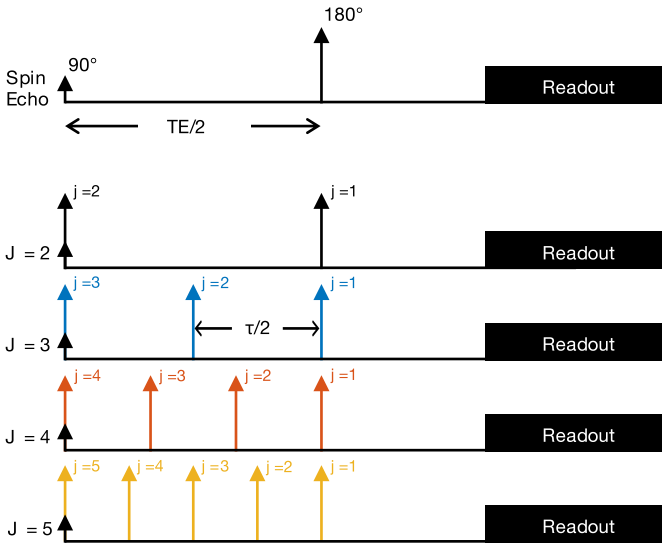

Fig. 2. In the asymmetric spin echo (ASE) pulse sequence the 180° refocusing pulse of a standard spin echo pulse sequence is shifted towards the 90° excitation pulse by a time τ/2. Values of τ were allowed to be equally distributed between τ=0 and τ=TE. In these examples 2 (black), 3 (blue), 4 (orange) or 5 (yellow) values of τ are acquired in separate repetitions to sample the decay of the R_2' weighted signal. R_2' is calculated by fitting these τ-weighted acquisitions with an exponential signal model. This placement scheme, as described by Eq. 3, was used to investigate the optimisation of ASE acquisition parameters for the measurement of R_2'. (For interpretation of the references to color in this figure legend, the reader is referred to the web version of this article.)

$$\tau_j=\left(\frac{j-1}{J-1}\right)TE \tag{3}$$

Multiple acquisitions with different values of τ can be fitted to measure R_2', where SNR per unit time is given by $\frac{R_2'}{\sqrt{J}\sigma_{R_2'}}$ and $\sigma_{R_2'}$ is the noise in the fitted value of R_2'. A $\frac{1}{\sqrt{J}}$ term is used in the SNR equation to penalise the increase in acquisition time that would result from increasing the number of τ values. For simplicity mono-exponential decay is assumed and the data is fitted using a weighted, linear, least squares fit. The signals, S_j, are linearised by setting $y_j=log_e(S_j)$ and if the noise in the image data is σ_0, then the noise in each linearised datapoint is $\sigma_j\approx\frac{\sigma_0}{S_j}$. The analytical solution for the error in the fit (Bevington and Robinson, 2003) gives Eq. (4).

$$\sigma_{R_2'}\approx\sqrt{\frac{1}{\Delta}\sum_{j=1}^{J}\frac{1}{\sigma_j^2}}\quad\text{where }\Delta=\sum_{j=1}^{J}\frac{1}{\sigma_j^2}\sum_{j=1}^{J}\frac{\tau_j^2}{\sigma_j^2}-\left(\sum_{j=1}^{J}\frac{\tau_j}{\sigma_j^2}\right)^2 \tag{4}$$

2.2. Modelling the qBOLD signal

Deoxygenated blood, present in blood vessel networks, causes additional MR signal decay due to the presence of MFGs that result from the difference in magnetic susceptibility between deoxyhaemoglobin and tissue. R_2' has been shown to be sensitive to such mesoscopic scale MFGs and an analytical solution has been presented to describe this relationship (Yablonskiy and Haacke, 1994). Here we present a generalised form of this equation as a function of deoxyhaemoglobin concentration, [dHb], and deoxygenated blood volume, DBV,

$$R_2'=DBV.\,\delta\omega=DBV.\,\gamma.\,\frac{4}{3}.\,\pi.\Delta\chi_0.\,\kappa.[dHb].B_0 \tag{5}$$

where δω is the characteristic frequency, γγ is the proton gyromagnetic ratio, $\Delta\chi_0$ is the susceptibility difference between fully oxygenated and fully deoxygenated red blood cells and κ is a conversion factor (κ=0.03) (Bain et al., 2006) enabling haemoglobin concentration, [Hb], to be calculated from haematocrit i.e. Hct=κ.[Hb]. Eq. (5) shows that a measure of R_2' contains information regarding the product of DBV and [dHb] scaled by known or assumed constants (γ, $\Delta\chi_0$, κ and B_0). However, to make a quantitative measure of brain oxygenation, [dHb] must be separated from DBV. Fortunately, the R_2'-weighted signal behaves differently in two different regimes of the parameter τ; the short and long τ regimes (see Fig. 1). The boundary between these regimes is typically considered to be at $T_c=1.5t_c$, where the characteristic time t_c is given as,

$$\frac{1}{t_c}=\delta\omega=\gamma.\,\frac{4}{3}.\,\pi.\Delta\chi_0.\,\kappa.[dHb].B_0 \tag{6}$$

For values of τ greater than $1.5t_c$ the tissue signal, s_t, is linearly exponential (Eq. 7a). However, for values of τ less than $1.5t_c$ the signal decays with a quadratic exponential profile (Eq. 7b). In both cases, R_2' decay is superimposed on the underlying R_2 decay of brain tissue, R_2^t.

$$s_t^L(\tau)=S(0).\exp[-TE.R_2^t].\exp[V]\exp[-\tau.\,DBV.\,\delta\omega]\qquad\tau>1.\,5t_c \tag{7a}$$

$$s_t^S(\tau)=S(0).\exp[-TE.R_2^t].\exp[-0.\,3.DBV.\,(\delta\omega.\,\tau)^2]\qquad\tau<1.\,5t_c \tag{7b}$$

Information regarding DBV can be extracted by comparing the linear and quadratic regimes represented by Eqs. (7a) and (7b), as shown in Eq.(8) and visualised in Fig. 1. It is important to note that these equations assume a static dephasing regime and therefore this model doesn't take into account the effects of diffusion narrowing.

$$DBV=log_e s_t^L(0)-log_e s_t^S(0) \tag{8}$$

Previously, a compartmental style model was introduced to better describe the brain tissue signal in terms of intravascular, extravascular and extracellular fluid components, Eq. (9) (He and Yablonskiy, 2007). The signals from tissue, extracellular fluid, consisting of cerebral spinal fluid (CSF) and interstitial fluid (ISF), and intravascular blood are represented by s_t, s_e and s_b respectively. λ and λ′ are the fractions of signal from CSF/ISF and blood, respectively, at a spin echo and are dependent on relaxation rates and spin densities of the tissue components as well as sequence timing parameters. The function F(τ) describes the τ dependent contribution of macroscopic field gradients.

$$S(\tau)=S_0.\,F(\tau).\,[(1-\lambda-\lambda').\,s_t+\lambda.\,s_e+\lambda'.s_b] \tag{9}$$

Eq. (10) describes the additional relaxation in the voxel due to the presence of CSF/ISF. Here R_2^e is the extracellular relaxation rate (i.e. relaxation due to CSF/ISF) and Δf is the frequency and offset of the CSF signal relative to bulk tissue water (Simon et al., 2016).

$$s_e(\tau)=S(0).\,\exp[-TE.R_2^e].\exp\,[-2.\pi.\,i.\Delta f.\,\tau] \tag{10}$$

Eq. (11) models the intravascular blood signal using an empirical relationship (Simon et al., 2016) based on blood relaxometry measurements (Zhao et al., 2007).

$$s_e(\tau)=S(0).\,\exp[-TE.R_2^b].\exp\,[-\tau.\,(R_2^{*b}-R_2^b)] \tag{11}$$

In the original implementation of qBOLD a large number of fitting parameters define the model resulting in a difficult optimisation problem. However, in the streamlined-qBOLD approach we aim to minimise the contributions of many of these compartments during image acquisition in order to simplify the model used for data analysis. Across all compartments the effect of R_2 related contributions is kept constant by using the ASE sequence, which uses the same TE for all values of τ and results in constant R_2-weighting for all images. The signal attenuation due to MFGs (F(τ)) is minimised by the GESEPI acquisition and the signal contribution from CSF is minimised through the use of a FLAIR preparation. Intravascular signal and the signal from ISF are not specifically addressed by the acquisition. However, since they represent small perturbations of the qBOLD signal they are neglected from the analysis model, thereby leaving only a single compartment described by Eqs. (7) and (8). The consequences of these assumptions are discussed later.

2.3. Measures of brain oxygenation

With measurements of R_2' and DBV made as described, a number of brain oxygenation measurements can be calculated by looking at the ratio of R_2' and DBV. Firstly, deoxyhaemoglobin concentration can be calculated without further subject specific information.

$$[dHb]=\frac{3.R_2'}{DBV.4.\gamma.\,\pi.\,\Delta\chi_0.\,\kappa.\,B_0} \tag{12}$$

With knowledge of the subject's haemoglobin concentration and under the assumption that arterial blood is fully saturated, the OEF can be calculated from [dHb] (Blockley et al., 2015).

$$OEF=\frac{[dHb]}{[Hb]} \tag{13}$$

Haemoglobin concentration can be inferred from haematocrit using κ. Haematocrit can be measured using venepuncture or more typically assumed to have a constant value, i.e. Hct=0.34 for small vessels like capillaries (Eichling et al., 1975). However, assuming a value of Hct like this means that this potential source of inter-subject variability isn't accounted for in the measurement of OEF. In contrast, calculating [dHb] using Eq. (12) does not require a measure of Hct.

3. Methods

3.1. FLAIR-GASE optimisation

The FLAIR preparation was optimised for a TR of 3 s and a typical CSF T_1 value of 3817 ms at 3 T (Lu et al., 2005) using Eq. (1). The

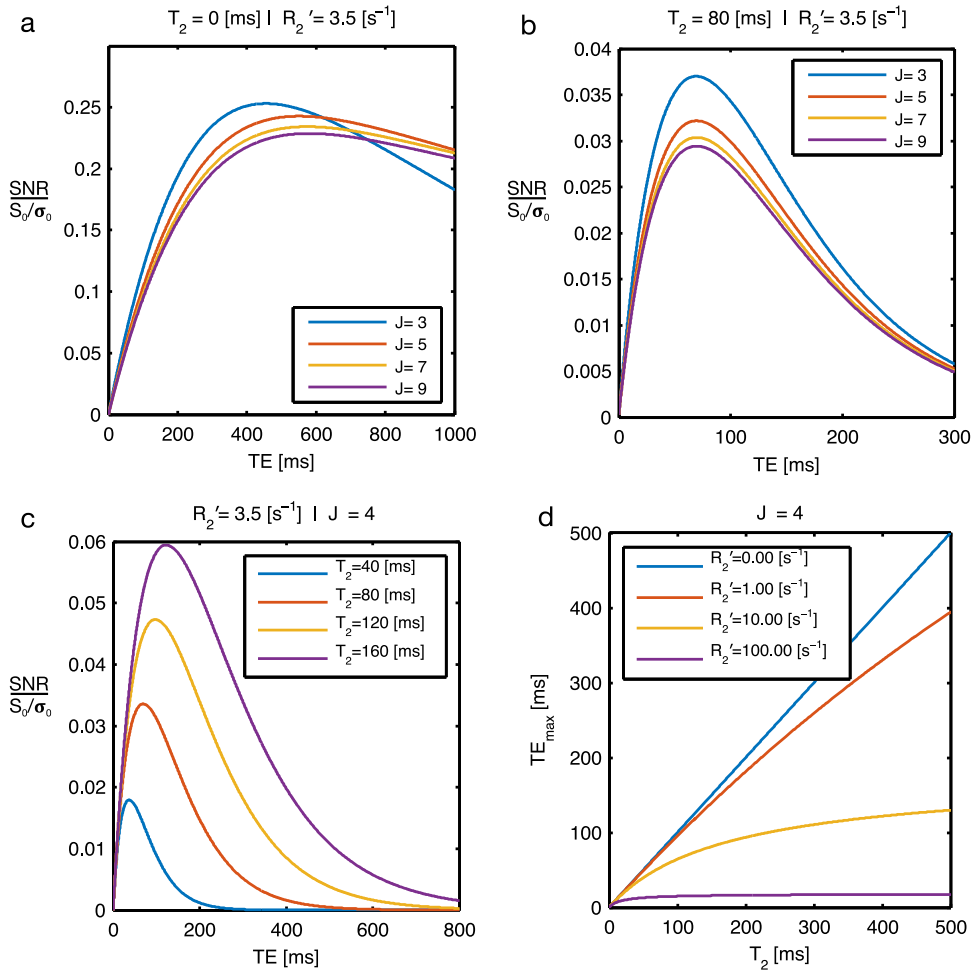

Fig. 3. ASE optimisation plots investigating the dependence of SNR on tissue T_2, echo time and number of τ-weighted sampling points. TE_{MAX} (the echo time at which R_2' is measured with maximum SNR) is shown to occur earlier when the effects of tissue T_2 are considered ((a) and (b)). TE_{MAX} is also shown to be dependent on underlying T_2 (c) and R_2' (d).

effect of ASE acquisition parameters (echo-time, tissue T_2 and number of τ-weighted sampling points) on measured R_2' SNR was investigated using Eqs. (2)–(4) outlined in the theory section. Calculations were performed in MATLAB, (Mathworks, Natick, MA).

3.2. Imaging

Seven healthy participants (aged 24–32; mean age 28 ± 3; 4 female: 3 male) were scanned using a 3 T TIM Verio system (Siemens Healthcare, Erlangen, Germany). Subjects were scanned under a technical development protocol agreed with local ethics and institutional committees. For comparison, two GASE scans were acquired with and without FLAIR preparation (TI_{FLAIR}=1210 ms). GASE acquisition parameters were FOV 240 mm^2, 64×64 matrix, ten 5 mm slices, TR/TE=3 s/74 ms, BW 2004 Hz/px. ASE images were acquired with τ=0, 16, 20, 24, 28, 32, 36, 40, 44, 48, 52, 56, 60 and 64 ms. This provided a spin-echo image with no R_2'-weighting (τ=0 ms) and R_2'-weighting in the mono-exponential regime (τ from 16 - 64 ms, (J = 13)), Eq. (7a) (Yablonskiy and Haacke, 1994). Each R_2'-weighted brain volume took 27 s to acquire, leading to a total acquisition time of 6 min 18 s for each GASE dataset. GESEPI is a multi-slab 3D acquisition whereby each 5 mm slab is phase-encoded in the z-direction into four 1.25 mm slices with 100% partition oversampling to reduce aliasing (total 8 k-space partitions). The four 1.25 mm slices of the slab are then averaged to produce a single 5 mm slice. Based on previous work we anticipate that the compensation provided by this GESEPI acquisition should enable 92% of through-plane MFGs to be corrected i.e. MFGs below the compensation threshold determined by the slice thickness will be corrected and those above will not (Blockley and Stone, 2016). Raw GASE imaging data were Tukey filtered prior to reconstruction. A high-resolution structural image was acquired if a recent image was not already available for a given subject (MPRAGE (Mugler and Brookeman, 1990): 192×192×174 matrix, resolution 1×1×1 mm^3, TR/TI/TE=2040/900/4.7 ms and flip angle 8°). This was used for registration of the functional data and generation of anatomically derived masks.

3.3. Data analysis

The four 1.25 mm slices of each slab were averaged to produce a single 5 mm slice. All GASE image τ-series were motion corrected using *MCFLIRT* (Jenkinson et al., 2002) to the spin echo image. The spin echo image was brain extracted using *3dAutomask* (Cox, 1996) to create a binary mask of the brain tissue and all remaining R_2'-weighted volumes were brain extracted using this mask. Further analysis of the brain extracted τ-series was performed in MATLAB (Mathworks, Natick, MA) where parameter maps were calculated for each ASE acquisition on a voxel-wise basis. R_2' was calculated using a weighted log-linear fit to the mono-exponential regime (τ ≥16 ms (Yablonskiy and Haacke, 1994)) of the ASE data (Fig. 1 and Eq. (3). From Eq. (6), T_c and OEF are inversely proportional. Using points in the mono-exponential regime of τ≥16 ms assumes a value of true OEF of 26% or higher. To ensure no points from the quadratic regime were included in the estimate of R_2' we favour overestimating T_c by underestimating the true OEF. The intercept of this fit and the spin-echo signal (τ=0 ms) were subtracted in order to provide a measure of DBV (Eq.(8)). OEF

and [dHb] were then calculated using Eqs. (12) and (13) where DBV and R_2' were measured and other parameters are known or assumed constants ($\Delta\chi_0$=0.264×10^{-6}, Hct=0.34) (He and Yablonskiy, 2007). This parameter estimation was performed for datasets with and without FLAIR CSF suppression (FLAIR-GASE and GASE, respectively) using the same model i.e. a model of the CSF compartment was not included for the GASE data. Subject specific ROI's of global grey matter were produced using FAST segmentation on the high-resolution structural images (Zhang et al., 2001) and registered to the native space of the GASE spin echo image using FLIRT (Jenkinson and Smith, 2001). The grey matter segmented masks were then thresholded at 0.6 to provide a binary mask. ROI measurements were taken from a subset of 6 adjacent slices to avoid areas with severe macroscopic field gradients lower in the brain.

4. Results

4.1. ASE optimisation

Fig. 3 demonstrates the effect of underlying tissue T_2 and ASE acquisition parameters (echo-time and number of τ-weighted sampling points) on measured R_2' SNR using Eqs. (2)–(4). In Fig. 3a–c normalised SNR (SNR/(S_0/σ_0)) of the fitted R_2' is shown to vary with echo time for ASE acquisitions. Fig. 3a shows this relationship when underlying tissue T_2 is ignored (T_2=0 ms). Fig. 3b shows this relationship for an underlying tissue T_2 of typical cortical grey matter (T_2=80 ms). In both figures R_2' was set to that of typical cortical grey matter (R_2' = 3.5 s^{-1}) and reproduced for a number of τ-weighted acquisitions (J). Comparing Fig. 3a to b it can be seen that the echo time at which the maximum SNR efficiency occurs (TE_{max}) is much shorter when underlying tissue T_2 is considered. Both R_2' and T_2 affect the time at which TE_{max} occurs. In Fig. 3b TE_{max} occurs at ~70 ms for all values of J. Fig. 3c demonstrates how tissue T_2 affects TE_{max}. As T_2 increases, the linear relationship between TE_{max} and T_2 breaks down.

Fig. 3d further investigates this relationship for varying values of R_2'. As R_2' approaches 0 s^{-1}, TE_{max} matches T_2. For larger values of R_2' this relationship becomes non-linear.

4.2. Demonstration of improved R_2' maps using FLAIR, CSF suppression

Fig. 4 shows example R_2' maps in a single subject, made using GASE (Fig. 4a) and FLAIR-GASE (Fig. 4b). A CSF partial volume map obtained from the FAST segmentation and registered to native spin-echo space is shown in comparison (Fig. 4c). R_2' maps made using GASE show areas of high R_2' which are minimised or reduced when CSF suppression is used (comparing Fig. 4a with b). Using the CSF partial volume maps for comparison (Fig. 5c), areas of high CSF partial volume correspond well with areas of high R_2' in the non-CSF suppressed acquisition (Fig. 5a) and these areas are minimised using CSF suppression (Fig. 5b).

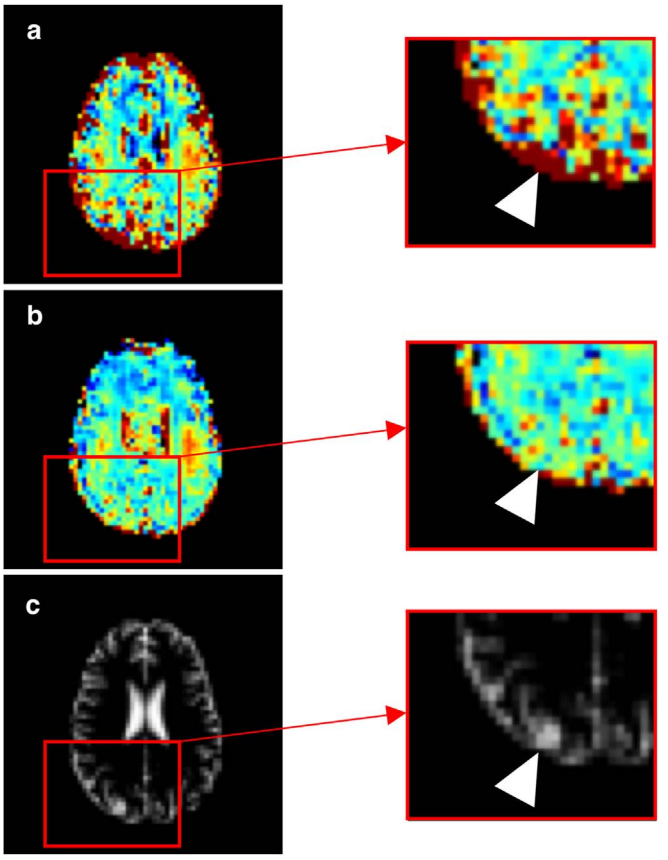

Fig. 5. Closer look at the effect of FLAIR CSF suppression on R_2'. Large areas of elevated R_2' can be seen in parameter maps acquired without FLAIR CSF suppression (a). These regions (white arrow) coincide with areas of high CSF volume as seen on the partial volume maps (c). These regions of elevated R_2' are significantly reduced with the application of FLAIR CSF suppression (b).

4.3. R_2' and DBV parameter maps

Fig. 6 shows parameter maps of R_2' (a), DBV (b), OEF (c) and [dHb] (d) presented alongside the spin echo image (e). The parameter maps were made using streamlined-qBOLD (FLAIR-GASE with qBOLD modelling) and displayed for an example subject. The OEF and [dHb] maps use the ratio of R_2' to DBV and are essentially scaled versions of each other. Table 1 compares GASE and FLAIR-GASE median (± interquartile range) parameter values across grey matter for each individual subject as well as group average values (mean ±

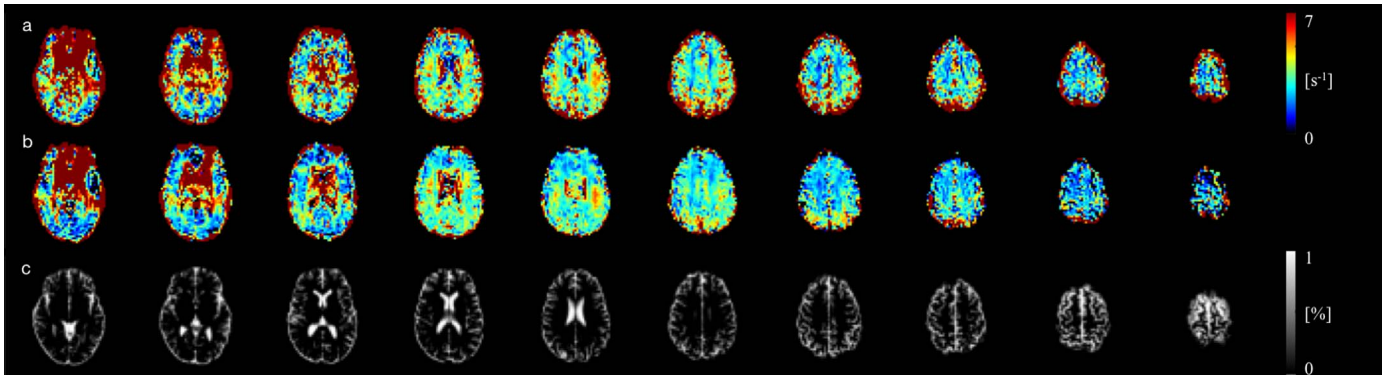

Fig. 4. Example R_2' parameter maps in a single subject calculated using GESEPI ASE without CSF suppression (a) and with CSF suppression (b). CSF partial volume map (c) estimated by segmenting a T_1 weighted anatomical image using FAST shows the regions of high CSF volume.

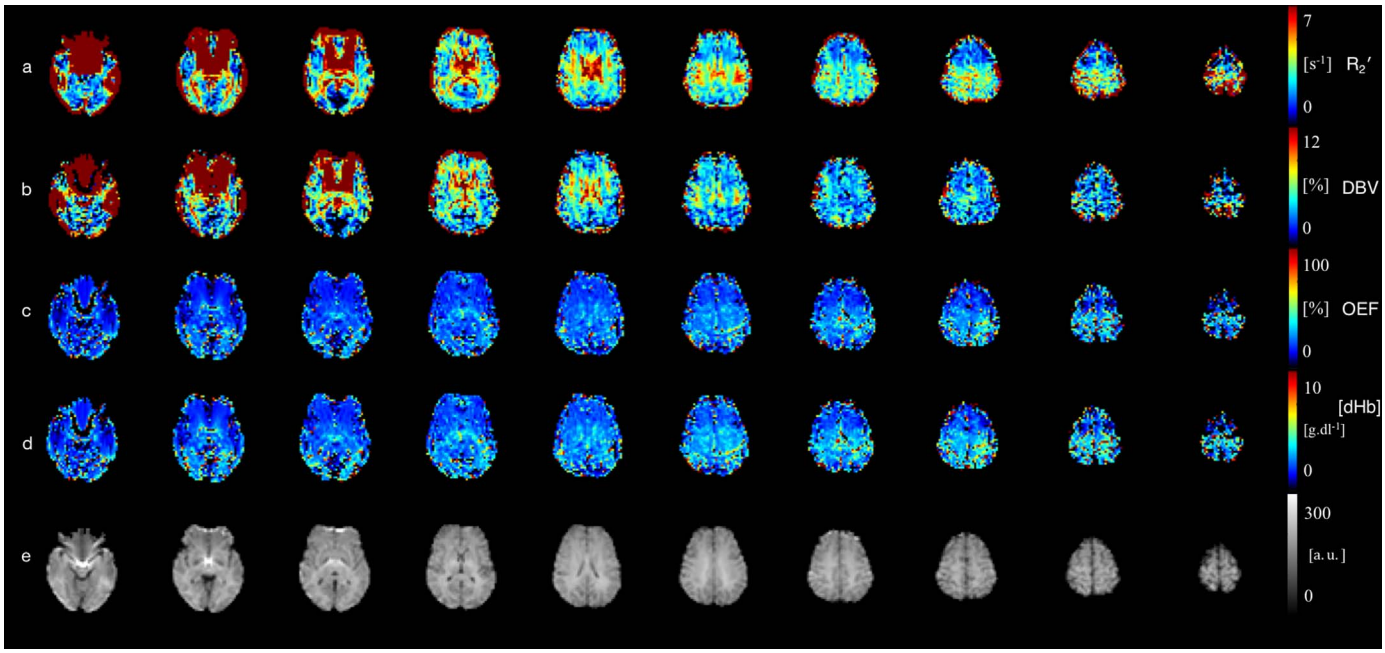

Fig. 6. Example parameter maps in a single subject calculated using FLAIR-GASE (a) R_2', (b) DBV, (c) OEF and (d) [dHb] presented alongside the spin-echo image (e). Note that OEF and [dHb] are scaled versions of each other.

standard deviation). R_2' and DBV can be seen to decrease significantly ($p < 0.001$ and $p < 0.01$, respectively) with the application of CSF nulling in a subject-wise manner.

Fig. 7 shows histograms of R_2', DBV, OEF and [dHb] voxel values contained within a grey matter ROI using FLAIR-GASE for subject 2 in Table 1. The distribution of R_2' and DBV are relatively normal as demonstrated by the small difference between the median (green line) and mean (red line) values. However, as OEF and [dHb] are calculated from the ratio of R_2' and DBV, outlying voxel values are introduced into the distribution. For OEF and [dHb] it appears, from Fig. 7, that the median better represents the peak of the voxel value distribution compared to the mean. As such, using the median to summarise the measurements made across global grey matter minimises the effect of outliers on the summary statistic and means that arbitrary thresholding of voxel values is not required.

For details on how to access the raw imaging data and simulation code that underpins these results please see Appendix A.

5. Discussion

Measurements of baseline brain oxygenation provide a unique insight into the metabolic integrity of brain tissue. As such imaging techniques capable of providing parametric maps of baseline brain oxygenation have important clinical and research applications. However, for these measurements to be truly useful it is important to have an imaging technique which is non-invasive, easy to perform and analyse, quick to acquire and robust. In this study a refinement of the qBOLD methodology is proposed in an attempt to progress this method towards a more streamlined measurement of baseline brain oxygenation. A novel acquisition protocol is used to remove confounding effects from the acquired MR signal, simplifying the application of the qBOLD model to the data and improving the robustness of the resultant baseline brain oxygenation parameter maps.

5.1. ASE optimisation

Through the optimisation framework it was found that measurements of R_2' have maximised SNR when TE is approximately equal to T_2. This result was found to be independent of J and true for values of R_2' and T_2 in healthy cortical grey matter (Wansapura et al., 1999). As such a TE of 74ms was chosen for the streamlined-qBOLD acquisition protocol.

Following from this, Fig. 3c shows that a mismatch between TE and target T_2 results in measuring R_2' with a suboptimal SNR. In disease, where underlying T_2 is globally or regionally altered, TE could be chosen to measure R_2' with maximum SNR for that target, assuming

Table 1
Individual values of brain oxygenation related parameters in global grey matter. Subject-wise values are given as the median ± interquartile range and the group average is given as the mean of these measures ± standard deviation. Statistical significant differences (two-tailed, paired t-test) between the group means of each of the parameters calculated using the FLAIR and no-FLAIR acquisitions were detected.

Subject #	R_2' [s^{-1}]		DBV [%]		OEF [%]		[dHb] [$g.dl^{-1}$]	
	FLAIR	*No FLAIR*	*FLAIR*	*No FLAIR*	*FLAIR*	*No FLAIR*	*FLAIR*	*No FLAIR*
1	2.9 ± 1.8	3.9 ± 3.3	3.6 ± 4.4	5.6 ± 3.7	22 ± 23	24 ± 15	2.5 ± 2.6	2.7 ± 1.7
2	2.9 ± 2.1	3.5 ± 2.9	4.4 ± 4.0	5.2 ± 4.9	20 ± 13	21 ± 17	2.3 ± 1.5	2.4 ± 1.9
3	2.2 ± 1.6	2.9 ± 2.6	3.0 ± 3.2	4.2 ± 3.5	21 ± 19	22 ± 14	2.4 ± 2.1	2.5 ± 1.6
4	2.6 ± 2.1	3.6 ± 2.6	3.5 ± 3.3	4.1 ± 3.3	23 ± 18	28 ± 19	2.6 ± 2.0	3.1 ± 2.2
5	2.6 ± 1.7	2.9 ± 2.3	3.8 ± 3.6	4.2 ± 3.1	21 ± 15	22 ± 15	2.4 ± 1.7	2.5 ± 1.7
6	3.0 ± 2.1	3.9 ± 3.2	3.3 ± 4.5	5.4 ± 4.3	22 ± 22	23 ± 14	2.5 ± 2.5	2.6 ± 1.6
7	2.1 ± 1.6	2.8 ± 2.5	3.4 ± 3.8	4.1 ± 4.1	18 ± 16	21 ± 20	2.0 ± 1.9	2.3 ± 2.3
Mean	**2.6 ± 0.4**	**3.4 ± 0.5**	**3.6 ± 0.4**	**4.7 ± 0.7**	**21 ± 2**	**23 ± 2**	**2.4 ± 0.2**	**2.6 ± 0.3**
Significance level	$p < 0.001$		$p < 0.01$		$p < 0.01$		$p < 0.01$	

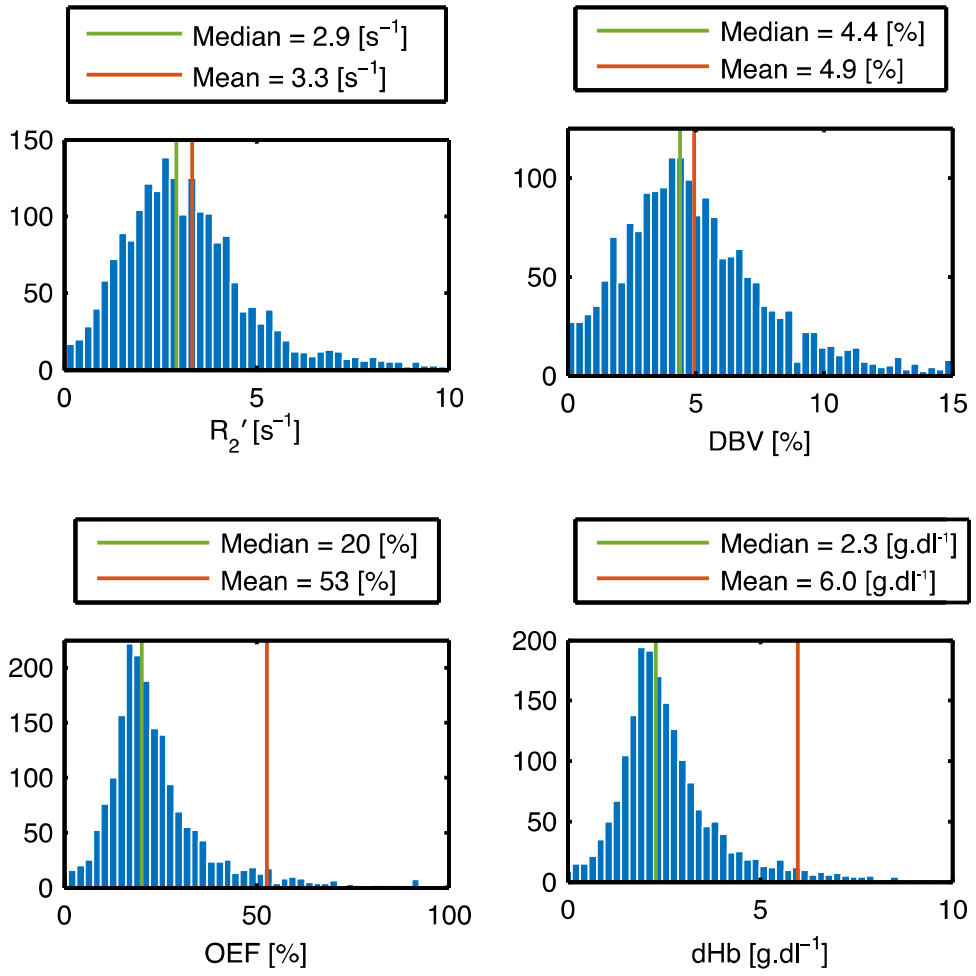

Fig. 7. Histograms of R_2', DBV, OEF and [dHb] in a region of grey matter for a sample subject made using FLAIR-GASE. Displayed results are for subject 2 from Table 1. The median (green line) better summarises the peak of the voxel distribution when compared to the mean (red line), particularly in the case of OEF and [dHb]. This justifies the use of medians as the subject-wise summary statistic in Table 1.

prior knowledge of T_2. In the case of regional changes in T_2 or even in healthy brain where tissues have a range of T_2, compromise must be made in terms of SNR.

Although the optimisation was performed to maximise the SNR efficiency of R_2' it can be interpreted in terms of OEF and DBV using Eqs. (5) and (12). In Fig. 3d varying values of R_2' ($\propto$ OEF.DBV) are investigated in relation to TE_{max} and target T_2. Assuming pathophysiological changes causing a range of OEF between 10 – 70% and assuming constant DBV (2%) this would lead to values of R_2' ranging from 0.8 s^{-1} to 5.5 s^{-1}. However pathophysiological changes in DBV are also likely and lead to a much greater range of R_2' such as that seen in Fig. 3d.

In practice minimum and maximum values of τ are determined by T_c and TE respectively. The value of T_c is dependent on OEF (Eq. (6)) and it has been suggested that overestimating T_c ensures sampling points from the quadratic regime aren't included in the estimate of R_2'. However, selection of an overly conservatively long T_c also leads to an increase in the minimum τ value and this directly scales the SNR efficiency, with T_c being inversely proportional to SNR efficiency.

In Fig. 3b SNR efficiency can be seen to decrease with increasing J. This is attributed to the use of SNR efficiency instead of SNR and the assumption of mono-exponential decay. SNR efficiency was chosen over SNR as minimising acquisition time is a central goal for this technique. The calculation of SNR efficiency involves an additional $\frac{1}{\sqrt{J}}$ term to penalise the addition of extra TRs that result from increasing J. By removing this $\frac{1}{\sqrt{J}}$ term, SNR increases with increasing J.

The R_2' signal was sampled using τ-weightings which were evenly distributed between the limits of τ_{min} and τ_{max} (T_c and TE) for a given J (Eq. (3)). The ASE optimisation suggests that repeatedly sampling only three values of τ should provide the highest SNR efficiency. However, in practice this doesn't allow for good characterisation of the exponential decay signal and as such the more practical sampling scheme in Eq. (3) was applied to data-collection alongside the maximum number of τ values that could be acquired within a given scan duration. Further improvements to the optimisation of the ASE acquisition could be made by incorporating the multicomponent decays described by the qBOLD model.

5.2. Demonstration of improved R_2' maps using CSF suppression

Motivated by earlier work to suppress CSF signal in Gradient Echo Sampling of Spin Echo (GESSE) based measurements of R_2' (Dickson et al., 2009; Simon et al., 2016), a FLAIR preparation was incorporated into the GASE pulse sequence. In Fig. 4 it can be seen that areas of high R_2' acquired without CSF suppression (Fig. 4a), correspond with areas of high CSF partial volume fraction (Fig. 4c) that are minimised by the application of a FLAIR preparation (Fig. 4b). Fig. 5 provides a closer inspection of these regions further demonstrating that superficially elevated R_2' in the non CSF suppressed maps coincide with regions of high CSF volume fraction. Values of R_2' without CSF suppression have been reported in the range of 2.7–3.8 s^{-1} (An and Lin, 2003; Blockley and Stone, 2016; Gelman et al., 1999; He and Yablonskiy, 2007; Ni et al., 2014). Simon et al. (2016) reported decreases in R_2' from 3.94 s^{-1} to 3.05 s^{-1} with the application of CSF suppression. These

values, although measured with a range of techniques (ASE, GESSE and GESFIDE), agree well with the trend of decreasing R_2' with CSF suppression seen in Table 1. From Table 1, it is also encouraging that despite the inherently lower SNR caused by the introduction of the FLAIR preparation pulse, the interquartile range of the R_2' measurements made using FLAIR GASE is consistently lower than that of the non-nulled GASE measurement.

Alongside this trend of decreasing R_2' it can also be seen that DBV decreases with the application of CSF suppression. These results can be explained by considering the following. From Eq. (10), the measured spin echo signal (τ=0) should not be influenced by the CSF signal compartment. As τ increases the signal measured using GASE is influenced by the signal from partial volumes of CSF, resulting in an apparent increase in R_2' for that volume. Extrapolating to zero causes the intercept to be higher in non-nulled data (no FLAIR) when compared with nulled data (FLAIR). As DBV is the difference between the measured spin echo and intercept of the fit to the linear regime (Eq. (8)) this should lead to higher DBV measurements made using non-nulled data in voxels with partial volumes of CSF. This evidence suggests that the application of CSF suppression offers a more reliable parametric mapping of R_2' and reduces the need to fit for CSF parameters in order to improve the power of the estimation of R_2' and DBV from the acquired signal.

5.3. R_2' and DBV parameter maps

Fig. 6a and b show example R_2' and DBV parameter maps in a second sample subject. The combination of these parameter maps is the basis for the quantitative brain oxygenation calculations performed later. As such it is important to investigate the pertinent features of these maps. From the R_2' relaxometry maps (Fig. 6a) it can be seen that areas of deep grey matter, known to have high iron content, correspond with areas of elevated R_2'. Furthermore, R_2' is observed to be elevated in white matter with respect to grey matter. Under the assumption that deoxyhaemoglobin is the dominant source of magnetic susceptibility, then we would expect a lower white matter R_2' since physiologically DBV is known to be lower than grey matter (Eq. (5)). However, we know that the myelin surrounding white matter tracts is diamagnetic and hence contributes an additional source of magnetic susceptibility. Likewise in maps of DBV (Fig. 6b), higher than expected values are seen in white matter possibly due to the high myelin content in this area. Therefore, we restrict further analysis to grey matter in this study.

5.4. Comparison of brain oxygenation measurements with the literature

The ratio of R_2' to DBV is used to calculate parametric maps of baseline brain oxygenation (Eqs. (12) and (13)). Table 2 presents previously published brain oxygenation related parameters for grey matter from a number of different techniques. From this table it can be seen that the measurement of DBV using FLAIR-GASE-qBOLD technique is high (3.6%), particularly in comparison to other MR based techniques (CBV_v=2.2% (Blockley et al., 2013a) and DBV=1.75% (He and Yablonskiy, 2007)).

There are several potential causes of the overestimation of DBV. Previously it has been shown that the use of flow dephasing gradients to remove intravascular signal reduces estimates of DBV (An and Lin, 2003). In addition, the qBOLD model assumes that protons are in the static dephasing regime. However, it has been shown that diffusion narrowing has a significant effect on R_2' weighted data and has led to overestimates of DBV acquired with the GESSE pulse sequence (Dickson et al., 2010; Pannetier et al., 2013). Simulations will be needed to investigate the effect of both intravascular signal and diffusion narrowing on the estimates of DBV made using the ASE pulse sequence and will inform the development of an improved qBOLD model.

Table 2
Literature values of brain oxygenation.

Method	DBV [%]	R_2' [s^{-1}]	OEF [%]
FLAIR-GASE-qBOLD	4.9 ± 0.5	3.3 ± 0.3	26 ± 2
ASE qBOLD (An and Lin, 2003)	~4-5	~3	30–40
qBOLD (He and Yablonskiy, 2007)	1.8 ± 0.1	2.9 ± 0.4	38 ± 2
GRE T_2* (Ulrich and Yablonskiy, 2015)	4.6 ± 0.1	5.1 ± 0.2	47.3
PET (Marchal et al., 1992)	–	–	~35-55
dual-calibrated FMRI (Bulte et al., 2012; Gauthier and Hoge, 2012; Wise et al., 2013)	–	–	29–50
Hyperoxia & BOLD (Blockley et al., 2013a)	2.2	–	–

Nonetheless, as a result of these high DBV measures and DBV being the denominator in Eqs. (11) and (12), lower brain oxygenation measurements are estimated using this technique (Table 1). From Table 1 group average values of [dHb] in grey matter are 2.4 ± 0.2 g .dl^{-1}. [dHb] in the blood is equivalent to the product of haemoglobin concentration ([Hb]) and OEF. The accepted levels of [Hb] for healthy adults is ~11.5–16.5 g .dl^{-1} for women and 13.0–17.5 g .dl^{-1} for men. Generally accepted literature values of OEF range from 25–50% for healthy brain. This indicates a [dHb] range of 2.9–8.8 g .dl^{-1}, suggesting the mean group value measured using the technique in this study is low.

Similarly, OEF values in Table 1 are considered to be on the low end of the spectrum for healthy grey matter. However, the spatial uniformity of the OEF maps is encouraging as OEF has been reported not to vary much across the brain (Gusnard and Raichle, 2001). Measures of brain oxygenation are particularly hard to validate using non-invasive means. The histograms of voxel values of OEF in global grey matter (Fig. 7) are particularly encouraging and demonstrate a clear peak. Extreme outlying voxel values in the OEF and [dHb] distribution were introduced by the use of DBV as the denominator in the calculation. As such medians were used to better summarise these distributions. Further identification of outlying voxels providing unreliable parameter estimates may be provided by interpreting these images alongside additional information such as magnetic field maps or errors in parameter fit. As such sources of systematic error leading to errors in scaling of the OEF and brain oxygenation measures warrant further investigation. Further validation of this brain oxygenation measure could be achieved by testing its sensitivity to changes in OEF with interventions that are known to alter it e.g. hypercapnia, hypocapnia or caffeine.

Elevated DBV is at least partly responsible for the low baseline brain oxygenation measurements seen in Table 1. Approaches for improving the measurement of DBV using qBOLD have already been discussed but an alternative implementation has suggested measuring blood volume using a separate technique to improve the accuracy of brain oxygenation measurements (Christen et al., 2012). In this multiparametric qBOLD approach DBV is measured using a dynamic susceptibility contrast (DSC) method that is sensitive to total blood volume. However, DBV in the qBOLD model refers specifically to the deoxygenated blood volume, a subset of the total blood volume, which

is difficult to directly localise and measure, and is largely situated on the venous side of the vasculature. Attempts have been made to measure DBV using hyperoxic contrast (Blockley et al., 2013a; Bulte et al., 2007), but these approaches haven't been combined with qBOLD so far. However, combining estimates of R_2' made in this study (2.6 s-1) with estimates of DBV made using hyperoxic contrast (2.2% (Blockley et al., 2013b)) produces an OEF estimate of 33% in cortical grey matter, suggesting this could be a promising approach.

It is also worth noting the effect of the constant terms in Eq. (12). In this study the generally accepted value of $\Delta\chi_0$ = 0.27 ppm (He and Yablonskiy, 2007; Spees et al., 2001) was used and resulted in a group OEF value of 21% in grey matter. In a previous ASE qBOLD implementation (An and Lin, 2003) an earlier estimate of $\Delta\chi_0$=0.18 ppm was used resulting in OEF values between 35% and 45% (Weisskoff and Kiihne, 1992). When scaled to a $\Delta\chi_0$ value of 0.27 ppm these values are reduced to between 23% and 30%. This demonstrates a level of consistency between similar ASE qBOLD implementations. Similarly, a value of Hct must be assumed or globally measured (i.e. obtained using venepuncture) in order to calculate a value of OEF. Assuming a value of Hct means a source of variation is not accounted for in the measurement of OEF. As a result, further validation of the constant Hct is warranted to improve the measurement of brain oxygenation.

5.5. Limitations and areas of future work

As part of the streamlining of the qBOLD approach a simple model of the qBOLD signal was used in this study. This has several limitations. Firstly, the stepwise approach to data analysis causes noise to be propagated along the analysis chain resulting in noisy estimates of OEF. Simultaneous estimation of DBV and OEF using a curve fitting approach would improve the noise properties in both estimates and allow the use of a model which smoothly transitions between the quadratic and linear exponential regimes (He and Yablonskiy, 2007). It would also remove the potential for bias due to spurious signals observed at the spin echo time (τ=0) in a previous study by acquiring a range of τ values in the quadratic exponential regime (He and Yablonskiy, 2007). Secondly, since the T_1 of ISF is likely to be shorter than that of CSF (He and Yablonskiy, 2007), the FLAIR preparation may not be effective in nulling its signal contribution. The impact of residual ISF signal on the brain oxygenation measurements is unknown and further work is required to understand its effect. Finally, in this study we have assumed that the intravascular blood has only a small effect on the qBOLD signal and can be neglected. It has previously been shown that intravascular signal may contribute to the overestimation of DBV and that flow dephasing gradients can be used to reduce this effect (An and Lin, 2003). Although this approach is shown to decrease the measured value of DBV in grey matter, it is difficult to dephase the signal from the slow flowing blood in the capillaries which make up approximately 40% of the cerebral blood volume (Weber et al., 2008). As such the addition of an intravascular signal model such as Eq. (11) combined with a curve fitting approach may be a more attractive approach. However, the introduction of such a model is not possible within the current analysis framework.

As stated above, in this study the GESEPI acquisition is predicted to correct for approximately 92% of through-plane macroscopic field gradients (Blockley and Stone, 2016). This level of correction is a compromise in order to minimise scan duration, whilst compensating for the majority of magnetic field gradients in the brain. From Figs. 4 and 6 it is clear that the GESEPI acquisition didn't provide sufficient correction in lower slices around the large MFGs in the frontal and temporal lobes. Specifically, MFGs greater than 147 μTm^{-1} will not be corrected at the maximum τ=64ms in the GASE implementation used in this study. This manifests as apparent elevations in R_2' in the lower three slices in these figures and is likely to make up the majority of the 8% of uncorrected voxels. An increase in the number, and a reduction in the thickness, of the slices of each slab would increase the maximum MFG that can be compensated. However, scan time will be increased and SNR reduced. Similarly in-plane MFGs can be reduced by increasing the in-plane resolution, albeit without the time penalty incurred by an increase in the number of slices in each slab (Blockley and Stone, 2016). Alternatively truncating the number of echoes used in the fitting of R_2', by examining the phase differences between adjacent voxels, could also enhance the robustness of this method (Storey et al., 2015). A combination of these approaches may allow improved compensation of magnetic field gradients in inferior slices.

The qBOLD approach used in this study to estimate brain oxygenation parameters, models MR signal formation that is influenced by susceptibility differences between blood in vessels and the brain tissue within which it is embedded. Other sources of susceptibility in the brain such as the myelin present in white matter or deposits of iron which can build up with ageing will cause inaccuracies in the resulting brain oxygenation quantifications as these susceptibility contributions are not accounted for in the qBOLD model. As the sequence used in this study is sensitive to these sources of susceptibility, whilst minimising contributions from CSF and macroscopic field inhomogenities, it could be used to investigate these sources as a potential form of contrast if combined with appropriate modelling or simulation of the signal formation. Further understanding of how these sources of susceptibility affect the MR signal would allow for these contributions to be accounted for in the qBOLD model improving the accuracy and precision of the brain oxygenation quantifications made using this approach, as demonstrated for white matter (Bouvier et al., 2013).

6. Conclusion

By minimizing known confounding effects during data acquisition it was possible to streamline the qBOLD technique with the aim of improving robustness without introducing undue complexity in either the acquisition or analysis. Streamlined qBOLD has the potential to provide parametric maps of brain oxygenation with good brain coverage, in clinically feasible times (< 7 min) and in a non-invasive, patient friendly manner without the need for external contrast. Further investigation is required to assess the sensitivity and reproducibility of these parametric measures and to compare this technique with more established techniques for global brain oxygenation estimation.

Appendix A. Supplementary data

The raw imaging data that underpins this work can be accessed via the Oxford Research Archive repository, doi: http://dx.doi.org/10.5287/bodleian:E24JbXQwO. In addition, simulation code used to optimise the ASE pulse sequence can be accessed via Zenodo, doi: http://dx.doi.org/10.5281/zenodo.168049.

Acknowledgements

This work was funded by EPSRC grant EP/K025716/1.

References

An, H., Lin, W., 2003. Impact of intravascular signal on quantitative measures of cerebral oxygen extraction and blood volume under normo- and hypercapnic conditions using an asymmetric spin echo approach. Magn. Reson. Med. 50, 708–716. http://dx.doi.org/10.1002/mrm.10576.

Bain, B.J., Lewis, S.M., Bates, I., 2006. Chapter 3 - Basic haematological techniques. (Dacie and Lewis Practical Haematology (Tenth Edition)In: Bates, S.M.L.J.B. (Ed.), Dacie and Lewis Practical HaematologyTenth Edition. Churchill Livingstone, Philadelphia, 25–57.

Bevington, P.R., Robinson, D.K., 2003. Data reduction and error analysis for the physical sciences 3rd ed.. McGraw-Hill, New York, NY. http://dx.doi.org/10.2307/27590662?ref=search-gateway:bb75c4114f9cb897ac56e3189a51421d.

Blockley, N.P., Griffeth, V.E.M., Germuska, M.A., Bulte, D.P., Buxton, R.B., 2013a. An analysis of the use of hyperoxia for measuring venous cerebral blood volume: comparison of the existing method with a new analysis approach. NeuroImage 72,

33–40. http://dx.doi.org/10.1016/j.neuroimage.2013.01.039.
Blockley, N.P., Griffeth, V.E.M., Germuska, M.A., Bulte, D.P., Buxton, R.B., 2013b. An analysis of the use of hyperoxia for measuring venous cerebral blood volume: comparison of the existing method with a new analysis approach. NeuroImage 72, 33–40. http://dx.doi.org/10.1016/j.neuroimage.2013.01.039.
Blockley, N.P., Griffeth, V.E.M., Stone, A.J., Hare, H.V., Bulte, D.P., 2015. Sources of systematic error in calibrated BOLD based mapping of baseline oxygen extraction fraction. NeuroImage 122, 105–113. http://dx.doi.org/10.1016/j.neuroimage.2015.07.059.
Blockley, N.P., Stone, A.J., 2016. Improving the specificity of R 2′ to the deoxyhaemoglobin content of brain tissue: prospective correction of macroscopic magnetic field gradients. NeuroImage 135, 253–260. http://dx.doi.org/10.1016/j.neuroimage.2016.04.013.
Borghammer, P., Cumming, P., Østergaard, K., Gjedde, A., Rodell, A., Bailey, C.J., Vafaee, M.S., 2012. Cerebral oxygen metabolism in patients with early Parkinson's disease. J. Neurol. Sci. 313, 123–128. http://dx.doi.org/10.1016/j.jns.2011.09.010.
Bouvier, J., Castellani, S., Debacker, C., Pannetier, N., Tropres, I., Krainik, A., Barbier, E. L., 2013. . Evaluation of multiparametric qBOLD in white matter: a simulation study, in:. Presented at the Proceedings of International Society of Magnetic Resonance in Medicine, Salt Lake City, Utah, USA. p. 2492.
Bulte, D., Chiarelli, P., Wise, R., Jezzard, P., 2007. Measurement of cerebral blood volume in humans using hyperoxic MRI contrast. J. Magn. Reson. Imaging 26, 894–899. http://dx.doi.org/10.1002/jmri.21096.
Bulte, D.P., Kelly, M., Germuska, M., Xie, J., Chappell, M.A., Okell, T.W., Bright, M.G., Jezzard, P., 2012. Quantitative measurement of cerebral physiology using respiratory-calibrated MRI. NeuroImage 60, 582–591. http://dx.doi.org/10.1016/j.neuroimage.2011.12.017.
Christen, T., Schmiedeskamp, H., Straka, M., Bammer, R., Zaharchuk, G., 2012. Measuring brain oxygenation in humans using a multiparametric quantitative blood oxygenation level dependent MRI approach. Magn. Reson. Med. 68, 905–911. http://dx.doi.org/10.1002/mrm.23283.
Christen, T., Zaharchuk, G., Pannetier, N., Serduc, R., Joudiou, N., Vial, J.-C., Rémy, C., Barbier, E.L., 2011. Quantitative MR estimates of blood oxygenation based on T2*: a numerical study of the impact of model assumptions. Magn. Reson. Med. 67, 1458–1468. http://dx.doi.org/10.1002/mrm.23094.
Cox, R.W., 1996. AFNI: software for analysis and visualization of functional magnetic resonance neuroimages. Comput. Biomed. Res. 29, 162–173.
Dickson, J.D., Ash, T.W.J., Williams, G.B., Harding, S.G., Carpenter, T.A., Menon, D.K., Ansorge, R.E., 2010. Quantitative BOLD: the effect of diffusion. J. Magn. Reson. Imaging 32, 953–961. http://dx.doi.org/10.1002/jmri.22151.
Dickson, J.D., Williams, G.B., Harding, S.G., Carpenter, T.A., Ansorge, R.E., 2009. . Nulling the CSF Signal in Quantitative fMRI, in:. Presented at the Proceedings of International Society of Magnetic Resonance in Medicine, Honolulu, Hawai'i, USA. p. 1640.
Eichling, J.O., Raichle, M.E., Grubb, R.L., Larson, K.B., Ter-Pogossian, M.M., 1975. In vivo determination of cerebral blood volume with radioactive oxygen-15 in the monkey. Circ. Res. 37, 707–714.
Gauthier, C.J., Hoge, R.D., 2012. Magnetic resonance imaging of resting OEF and CMRO2 using a generalized calibration model for hypercapnia and hyperoxia. NeuroImage 60, 1212–1225. http://dx.doi.org/10.1016/j.neuroimage.2011.12.056.
Gelman, N., Gorell, J.M., Barker, P.B., Savage, R.M., Spickler, E.M., Windham, J.P., Knight, R.A., 1999. MR imaging of human brain at 3.0 T: preliminary report on transverse relaxation rates and relation to estimated iron content. Radiology 210, 759–767. http://dx.doi.org/10.1148/radiology.210.3.r99fe41759.
Gowland, P.A., Bowtell, R., 2007. Theoretical optimization of multi-echo fMRI data acquisition. Phys. Med. Biol. 52, 1801–1813. http://dx.doi.org/10.1088/0031-9155/52/7/003.
Gusnard, D.A., Raichle, M.E., 2001. Searching for a baseline: functional imaging and the resting human brain. Nat. Rev. Neurosci. 2, 685–694. http://dx.doi.org/10.1038/35094500.
Hajnal, J.V., Decoene, B., Lewis, P.D., Baudouin, C.J., Cowan, F.M., Pennock, J.M., Young, I.R., Bydder, G.M., 1992. High signal regions in normal white matter shown by heavily T2-weighted csf nulled Ir sequences. J Comput. Assist Tomogr. 16, 506–513.
He, X., Yablonskiy, D.A., 2007. Quantitative BOLD: mapping of human cerebral deoxygenated blood volume and oxygen extraction fraction: default state. Magn. Reson Med 57, 115–126. http://dx.doi.org/10.1002/mrm.21108.
Ishii, K., Kitagaki, H., Kono, M., Mori, E., 1996. Decreased medial temporal oxygen metabolism in Alzheimer's disease shown by PET. J. Nucl. Med. 37, 1159–1165.
Ito, H., Ibaraki, M., Kanno, I., Fukuda, H., Miura, S., 2005. Changes in cerebral blood flow and cerebral oxygen metabolism during neural activation measured by positron emission tomography: comparison with blood oxygenation level-dependent contrast measured by functional magnetic resonance imaging. J Cereb. Blood Flow. Metab. 25, 371–377. http://dx.doi.org/10.1038/sj.jcbfm.9600030.
Jenkinson, M., Bannister, P., Brady, M., Smith, S., 2002. Improved optimization for the robust and accurate linear registration and motion correction of brain images. NeuroImage 17, 825–841.
Jenkinson, M., Smith, S., 2001. A global optimisation method for robust affine registration of brain images. Med Image Anal. 5, 143–156.
Leenders, K.L., 1994. PET: blood flow and oxygen consumption in brain tumors. J Neurooncol 22, 269–273.
Lu, H., Nagae-Poetscher, L.M., Golay, X., Lin, D., Pomper, M., van Zijl, P.C.M., 2005. Routine clinical brain MRI sequences for use at 3.0 T. J. Magn. Reson. Imaging 22, 13–22. http://dx.doi.org/10.1002/jmri.20356.
Marchal, G., Rioux, P., Petit-Taboué, M.C., Sette, G., Travère, J.M., Le Poec, C., Courtheoux, P., Derlon, J.M., Baron, J.C., 1992. Regional cerebral oxygen consumption, blood flow, and blood volume in healthy human aging. Arch. Neurol. 49, 1013–1020. http://dx.doi.org/10.1001/archneur.1992.00530340029014.
Mugler, J.P., Brookeman, J.R., 1990. Three-dimensional magnetization-prepared rapid gradient-echo imaging (3D MP RAGE). Magnetic Resonance. Medicine 15, 152–157. http://dx.doi.org/10.1002/mrm.1910150117.
Ni, W., Christen, T., Zun, Z., Zaharchuk, G., 2014. Comparison of R2′ measurement methods in the normal brain at 3 T. Magn. Reson. Med. 73, 1228–1236. http://dx.doi.org/10.1002/mrm.25232.
Pannetier, N.A., Sohlin, M., Christen, T., Schad, L., Schuff, N., 2013. Numerical modeling of susceptibility-related MR signal dephasing with vessel size measurement: phantom validation at 3T. Magn. Reson. Med. 72, 646–658. http://dx.doi.org/10.1002/mrm.24968.
Shen, Y., Kauppinen, R.A., Vidyasagar, R., Golay, X., 2009. A functional magnetic resonance imaging technique based on nulling extravascular gray matter signal. J. Cereb. Blood Flow. amp; Metab. 29, 144–156. http://dx.doi.org/10.1038/jcbfm.2008.96.
Simon, A.B., Dubowitz, D.J., Blockley, N.P., Buxton, R.B., 2016. A novel Bayesian approach to accounting for uncertainty in fMRI-derived estimates of cerebral oxygen metabolism fluctuations. NeuroImage 129, 198–213. http://dx.doi.org/10.1016/j.neuroimage.2016.01.001.
Song, R., Song, H.K., 2007. Echo-spacing optimization for the simultaneous measurement of reversible (R2') and irreversible (R2) transverse relaxation rates. Magn. Reson. Imaging 25, 63–68. http://dx.doi.org/10.1016/j.mri.2006.09.008.
Spees, W.M., Yablonskiy, D.A., Oswood, M.C., Ackerman, J.J., 2001. Water proton MR properties of human blood at 1.5 T: magnetic susceptibility, T(1), T(2), T*(2), and non-Lorentzian signal behavior. Magnetic Resonance. Medicine 45, 533–542.
Storey, P., Lui, Y.W., Novikov, D.S., 2015. . Artifact-free T2* mapping without post hoc corrections, in:. Presented at the Proceedings of the International Society of Magnetic Resonance in Medicine, Toronto, Ontario, Canada, p. 442.
Ulrich, X., Yablonskiy, D.A., 2015. Separation of cellular and BOLD contributions to T2* signal relaxation. Magn. Reson. Med. N./a–N./a. http://dx.doi.org/10.1002/mrm.25610.
Wansapura, J.P., Holland, S.K., Dunn, R.S., Ball, W.S., 1999. NMR relaxation times in the human brain at 3.0 T. J. Magn. Reson. Imaging 9, 531–538. http://dx.doi.org/10.1002/(SICI)1522-2586(199904)9:4 < 531::AID-JMRI4 > 3.0.CO;2-L.
Weber, B., Keller, A.L., Reichold, J., Logothetis, N.K., 2008. The microvascular system of the striate and extrastriate visual cortex of the macaque. Cereb. Cortex 18, 2318–2330. http://dx.doi.org/10.1093/cercor/bhm259.
Weisskoff, R.M., Kiihne, S., 1992. MRI susceptometry: image-based measurement of absolute susceptibility of MR contrast agents and human blood. Magn. Reson Med 24, 375–383. http://dx.doi.org/10.1002/mrm.1910240219.
Wise, R.G., Harris, A.D., Stone, A.J., Murphy, K., 2013. Measurement of OEF and absolute CMRO2: mri-based methods using interleaved and combined hypercapnia and hyperoxia. NeuroImage 83, 135–147. http://dx.doi.org/10.1016/j.neuroimage.2013.06.008.
Wismer, G.L., Buxton, R.B., Rosen, B.R., Fisel, C.R., Oot, R.F., Brady, T.J., Davis, K.R., 1988. Susceptibility Induced Mr Line Broadening - Applications to Brain Iron Mapping. J Comput. Assist Tomogr. 12, 259–265.
Yablonskiy, D.A., 1998. Quantitation of intrinsic magnetic susceptibility-related effects in a tissue matrix. Phantom Stud. Magn. Reson. Med. 39, 417–428.
Yablonskiy, D.A., Haacke, E.M., 1994. Theory of NMR signal behavior in magnetically inhomogeneous tissues: the static dephasing regime. Magn. Reson. Med., 1–15.
Yablonskiy, D.A., Sukstanskii, A.L., He, X., 2013. Blood oxygenation level-dependent (BOLD)-based techniques for the quantification of brain hemodynamic and metabolic properties - theoretical models and experimental approaches. NMR Biomed. 26, 963–986. http://dx.doi.org/10.1002/nbm.2839.
Yamauchi, H., Fukuyama, H., Nagahama, Y., Nabatame, H., Nakamura, K., Yamamoto, Y., Yonekura, Y., Konishi, J., Kimura, J., 1996. Evidence of misery perfusion and risk for recurrent stroke in major cerebral arterial occlusive diseases from PET. J. Neurol., Neurosurg. Psychiatry 61, 18–25. http://dx.doi.org/10.1136/jnnp.61.1.18.
Yang, Q.X., Williams, G.D., Demeure, R.J., Mosher, T.J., Smith, M.B., 1998. Removal of local field gradient artifacts in T-2*-weighted images at high fields by gradient-echo slice excitation profile imaging. Magn. Reson. Med. 39, 402–409. http://dx.doi.org/10.1002/mrm.1910390310.
Zhang, Y.Y., Brady, M., Smith, S., 2001. Segmentation of brain MR images through a hidden Markov random field model and the expectation-maximization algorithm. IEEE Trans. Med Imaging 20, 45–57. http://dx.doi.org/10.1109/42.906424.
Zhao, J.M., Clingman, C.S., Närväinen, M.J., Kauppinen, R.A., van Zijl, P.C.M., 2007. Oxygenation and hematocrit dependence of transverse relaxation rates of blood at 3 T. Magn. Reson. Med. 58, 592–597. http://dx.doi.org/10.1002/mrm.21342.